5-1-1999

Semiempirical *R*-matrix theory of low energy electron–CF_3Cl inelastic scattering

R. S. Wilde
University of Nebraska-Lincoln

Gordon A. Gallup
University of Nebraska-Lincoln, ggallup1@unl.edu

Ilya I. Fabrikant
University of Nebraska-Lincoln, ifabrikant@unl.edu

Published in *Journal of Physics B: Atomic, Molecular and Optical Physics* **32** (1999), pp. 663–673. http://www.iop.org/EJ/journal/JPhysB

Semiempirical *R*-matrix theory of low energy electron–CF_3Cl inelastic scattering

R. S. Wilde, G. A. Gallup, and I. I. Fabrikant
Department of Physics and Astronomy, University of Nebraska–Lincoln, Lincoln, NE 68588-0111

Submitted September 1998; revised November 1998.

Abstract. We apply a semiempirical *R*-matrix theory to calculations of vibrational excitation and dissociative attachment in the CF_3Cl molecule for electron energies below about 3 eV. We employ two sets of model parameters corresponding to two different forms of the CF_3Cl^- potential curve. We find that our present, *ab initio* calculated anion curve gives vibrational excitation and dissociative attachment cross sections in good agreement with experimental measurements. We also compare the results of our theory with those of a recently published classical theory.

1. Introduction

Recent years have seen a number of papers reporting work on the scattering of low energy electrons from the CF_3Cl molecule. Both experimental [1–8] and theoretical [9, 10] studies are represented. This focus arises from the importance of dissociative attachment (DA) in CF_3Cl to the practical applications [11] of plasma etching, gas discharge plasmas, negative ion sources, and other similar processes. In particular, the introduction of small amounts of halofluorocarbons such as CF_3Cl can influence the efficiency of the CF_4 etching plasma through the production of Cl^- ions [4].

At low electron energies the main processes other than elastic scattering from CF_3Cl are DA and vibrational excitation (VE). The previous theoretical studies have been restricted to classical treatments of DA. In this paper we present a quantum mechanical treatment of DA and VE. These processes mainly involve the C–Cl bond in the molecule, and we follow closely our previous treatments of DA and VE in the similar molecules CH_3Cl [12–14] and C_2H_5Cl [15], extending our model to include CF_3Cl. We compare our results with experimental measurements and with the classical theory of Lehr *et al.* [9, 10].

DA cross sections are quite often very sensitive to the experimental environment. In particular, the gas phase cross sections for CF_3Cl are very sensitive to temperature [1]. Also, experiments and calculations have shown a large increase in the DA cross sections when a DA species is placed on a surface or in a bulk medium [16–20]. Our present gas phase calculation can provide a basis for extending our model to study such phenomena for CF_3Cl.

For incident electron energies below about 3 eV the inelastic scattering in CF_3Cl is dominated by a resonance due to the σ^* LUMO (lowest unoccupied molecular orbital) of CF_3Cl. The temporary negative ion associated with this state excites mainly the ν_3 C–Cl stretching mode of CF_3Cl and produces Cl^- ions as the main dissociation product for these low electron energies [1]. A broad feature centered at 2 eV due to this resonance is observed in the total scattering cross section [5] and in the VE cross section from the ground state [2]. Due to the short lifetime of the temporary anion,

only that part of the nuclear wavepacket that is near the right edge of the Franck–Condon region will survive to reach the crossing point of the neutral and anion curves and will contribute significantly to DA. This causes the peak in the DA cross section to shift downward from the peak in the VE to about 1.4 eV. Interesting temperature effects have also recently been observed by Hahndorf *et al.* [1] in the DA cross section of CF_3Cl. They find that as the temperature rises the peak in the cross section shifts from about 1.4 eV to 1.1 eV, approximately doubles in magnitude, and broadens slightly. A dramatic rise in the DA cross section is also observed at the 0 eV threshold as the temperature rises from 300 to 800 K. These effects can be explained by the higher contribution to the DA cross section of higher vibrational states at higher temperatures.

Similar temperature effects are observed in CH_3Cl [14, 15]. This is expected since the LUMO of CH_3Cl is also σ^*, and at low energies the C–Cl bond is mainly affected. We have previously calculated VE and DA cross sections for CH_3Cl using the present *R*-matrix model [12, 13], and here we extend the procedure to consider VE and DA in CF_3Cl.

This paper is organized as follows. In section 2 we describe our theoretical model and the method for obtaining the empirical parameters of the model. In sections 3 and 4 we present our results for VE and DA and compare them both with existing experimental and theoretical results. Section 5 is a brief conclusion.

2. Theoretical model

We use the semiempirical, *R*-matrix model, described in more detail in [12, 13], to calculate the VE and DA cross sections for CF_3Cl. In this model the single pole approximation [21] is used to describe the *R*-matrix in the fixed-nuclei approximation.

$$R(\rho) = \frac{\gamma^2(\rho)}{W(\rho) - E_e} + R_b, \tag{1}$$

where $W(\rho)$ is the *R*-matrix eigenvalue, E_e the electron energy, ρ the internuclear distance and R_b a background term which is assumed to be independent of E_e and ρ. $W(\rho)$is defined as

$$W(\rho) = U(\rho) - V(\rho), \tag{2}$$

where $U(\rho)$ is the potential energy of the negative ion and $V(\rho)$ that of the neutral molecule. We represent these potentials by the Morse functions

$$U(\rho) = Be^{-2\beta\rho} - Ce^{-\alpha\rho} + D, \tag{3}$$

$$V(\rho) = A(e^{-2\alpha\rho} - 1)^2. \tag{4}$$

The function $\gamma(\rho)$ in the *R*-matrix is also parametrized as

$$\gamma(\rho) = \gamma_0 + \frac{\gamma_1}{e^{\zeta\rho} + \eta}. \tag{5}$$

These parameters are obtained by fitting the calculated VE cross section for the $v = 0 \rightarrow 1$ transition to the experimental data of Mann and Linder [2]. We note that the transition dipole moment of CF_3Cl is nearly zero [22] so only the resonant scattering amplitude is important in calculating the differential VE cross sections, see [13]. In order to calculate DA cross sections, the nuclear dynamics must be incorporated. We do this by replacing the denominator in equation (1) by the operator $H_I - E$, [23] where E is the total energy and H_I is the negative ion Hamiltonian, which includes the kinetic energy operator. The basic matching equation of the *R*-matrix theory becomes an integral equation, and this is solved using the quasiclassical method [24, 25]. The coefficients of the inte-

Table 1. Parameters of the *R*-matrix theory, in au.

	β	B	C	D	γ_0	γ_1	ζ	η	R_b
Model 1	0.884	0.1879	0.1198	0.005 414	0.072	0.118	5.0	0.225	0.6
Model 2	0.82	0.0928	0.009	−0.011	0.08	0.102	3.8	0.3	0.42

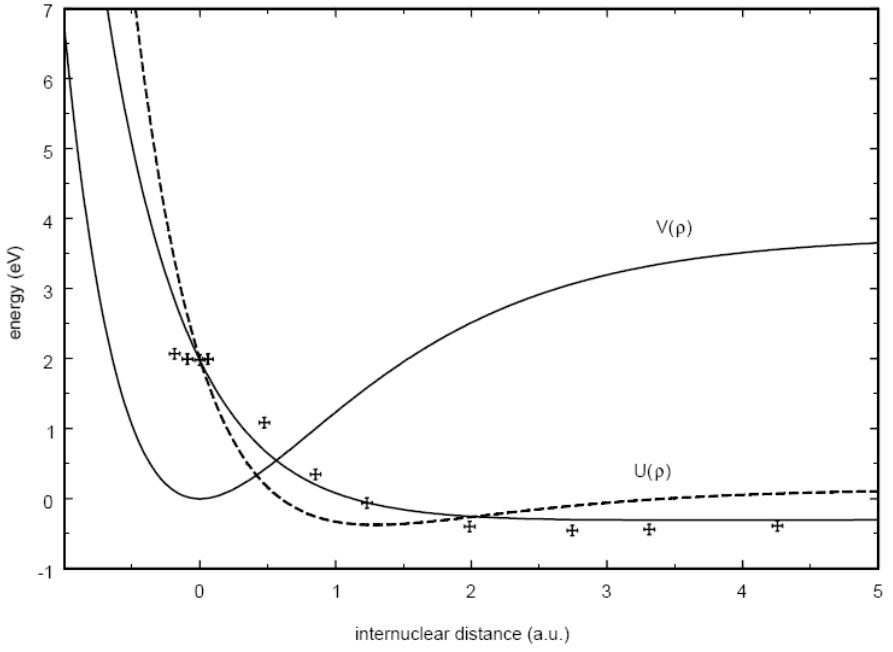

Figure 1. Potential curves of the problem. Curve $V(\rho)$, potential curve for the neutral molecule; crosses, calculated points on the curve $U(\rho)$ (see section 2 for description of the curves). Curve $U(\rho)$, anion potential curve; solid curve, curve fitted to our calculated points; dashed curve, from [1].

gral equation depend on the electron wavefunction's values on the *R*-matrix sphere in different vibrational channels. These are obtained by inward integration of the Schrödinger equation that includes only the long range dipole and spherical polarization interactions. The radius of the *R*-matrix sphere was taken to be 4 au.

The two models of Table 1 correspond to the use, in our calculations, of two different parameter sets for the negative ion potential curve, $U(\rho)$. In model 1 we have used the potential function published in [1] and in model 2 we have fitted the Morse parameters to an *ab initio* calculation of the potential curves. The potential curves are shown in Figure 1.

The *ab initio* calculation for CF_3Cl^- was carried out using the GAMESS [26] program with a 6-31G[d] basis in which the S–P subshells used different Gaussian scale factors. The latter is a standard option of GAMESS. The geometry was optimized using the ROHF (restricted open-shell Hartree–Fock) energy, constraining the ion to have C_{3v} symmetry and a fixed C–Cl distance. As noted by Asubiojo *et al.* [27], CF_3Cl^- forms a sufficiently stable state to be observed in an ion cyclotron resonance spectrometer. Hahndorf *et al.* [1] use a dissociation energy for this of 0.52 eV, a value reflected in the curve of model 1. The *ab initio* calculation, not surprisingly, gives the smaller value of 0.24 eV. We expect there to be three main contributions to the attraction. The CF_3 radical

possesses a dipole moment of ≈ 0.7 debye in our calculation, and its orientation is such that there is attraction to the Cl^- ion. The ion charge will induce a further dipole in the radical to give an attractive interaction. Van der Waals attraction will also occur between the two parts of the system. Only the first two of these can be present in our ROHF calculation. Ion-induced dipole interactions are frequently reproduced however, to only 30–60% of true values with AO bases similar to the one we used. An experimental value for the polarizability of the CF_3 radical is apparently unknown. Bertran *et al.* [28] have also given a calculation of the negative ion curve for CF_3Cl^-. They too find that the energy at the crossing with the neutral molecule curve occurs at a higher energy than that of model 1. We discuss this more fully below.

At short C–Cl distances our calculation shows a variational collapse, since, of course, inside the crossing point the negative ion state is really a resonance and part of the continuum.

Morse parameters giving an exact fit to the calculated points cannot be determined, since the Morse potential necessarily falls off exponentially with distance while the energies of the calculated points fall off as ρ^{-2}. Nevertheless, the main features are reproduced, particularly in the critical region around the crossing point. The potential function that we used for the neutral molecule is the same for both of our models and was taken from [1].

There are two major differences between the model potential curves. The calculated curve passes through the Franck–Condon region less steeply than the curve of model 1. This, as pointed out in [9], will have the effect of decreasing the DA cross sections, since, classically speaking, the nuclei will spend more time in reaching the crossing point of the neutral and anion curves. Therefore, the system will have a larger probability of autoionizing before stabilizing and dissociating. In addition, the crossing point for the model 2 potential occurs at a higher energy and this will also tend to reduce the DA cross sections. If the crossing occurs at a higher energy the lower vibrational levels will not contribute as much to the DA cross section and the temperature-averaged DA cross sections will consequently be smaller than if the crossing occurs at a lower energy.

3. Vibrational excitation

In Figure 2 we show the differential VE cross sections at a scattering angle of 90° for CF_3Cl. We have fit these cross sections for both models 1 and 2 to the experimental results of Mann and Linder [2] for the excitation of the ν_3 stretching mode. A better fit is obtained using model 2, which corresponds to use of the *ab initio* calculation of the anion curve. The rise of the experimental cross section at higher energies is possibly due to a higher-lying resonance state not included in our calculations.

In Figures 3 and 4 we compare our calculations of the angle integrated VE cross sections for CF_3Cl with the classical theory presented by Lehr *et al.* [10]. Figure 3 shows cross sections for the representative transitions from the initial vibrational state $\nu_i = 3$ to $\nu_f = 4$ and 5. In the classical cross sections two maxima occur at energies which correspond to the classical turning points. Our calculations show oscillations in the cross sections throughout the range of the classically allowed motion. These differences are due to the different probability distributions of the nuclear motion used in the two models. The classical calculations use a classical distribution so the nuclei should be expected in this model to spend more time near the classical turning points than in the centre of the Franck–Condon region. Our calculations use a quantum mechanical probability distribution, which, of course, depends upon the wavefunction for the nuclear motion. Using the quasiclassical

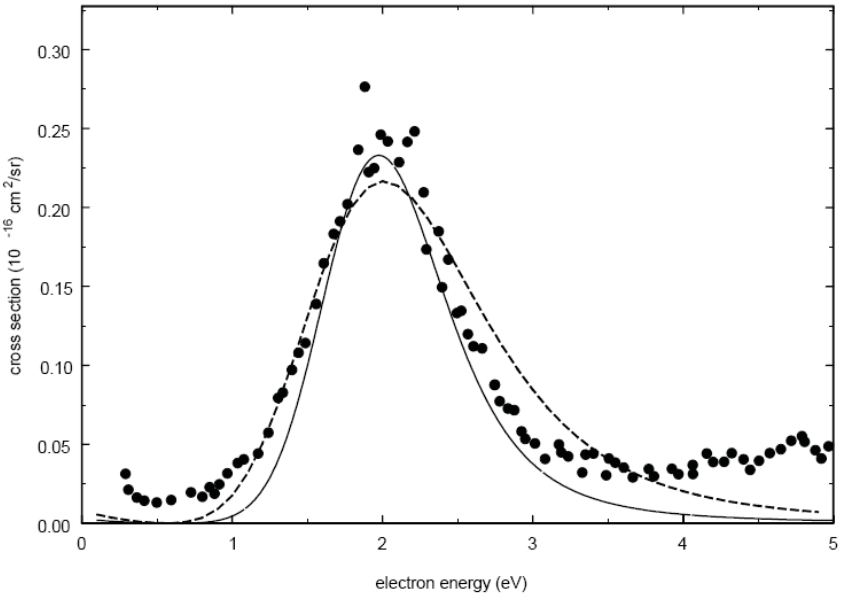

Figure 2. Differential VE cross section for the CF_3Cl molecule at a scattering angle of $\theta = 90°$. Circles, experimental data of [2]; dashed and solid curves, present calculations with the parameters of models 1 and 2, respectively.

approximation [24] we can write the expression for the VE cross sections as

$$\sigma_{i\to f} = \frac{v_f}{v_i}\frac{1}{8\pi^3}\frac{(I_i)^2(I_f)^2}{Q^2}, \tag{6}$$

where I_i and I_f are generalized Franck–Condon factors between the nuclear wavefunction in the anion state and the initial and final vibrational wavefunctions of the neutral molecule, respectively. Q is the resonance denominator. If the resonance is wide, the energy dependence of the cross section will be dominated by oscillations in the Franck–Condon factors, which reflect the oscillations in the nuclear wavefunctions. For a narrow resonance the resonant denominator will cause the cross sections to have a familiar Breit–Wigner shape. So the major difference between the classical model and our model is the different probability distribution for the nuclear motion. We note also that the calculations of [9, 10] have used the anion potential of Hahndorf *et al.* [1] only, so the classical theory might give different results if another form of the anion curve were used.

In Figure 4 we compare our calculations of the angle integrated VE cross sections from the ground state summed over the first 12 excited vibrational states with the classical calculations. The classical model gives a peak magnitude which is about half that of the *R*-matrix calculations. This is again due to the different nuclear probability distributions [9, 10]. Mann and Linder [2] have estimated the magnitude of this cross section to be about 5×10^{-16} cm^2. Since the cross sections for excited states greater than $v_f = 12$ are small and do not appreciably change the summed cross sections of Figure 4, we see that our calculations are only slightly larger than this experimental estimate, whereas the classical calculations are about half the experimentally estimated value. We also note here that the peak in the integrated VE cross sections occurs at energies below 2 eV.

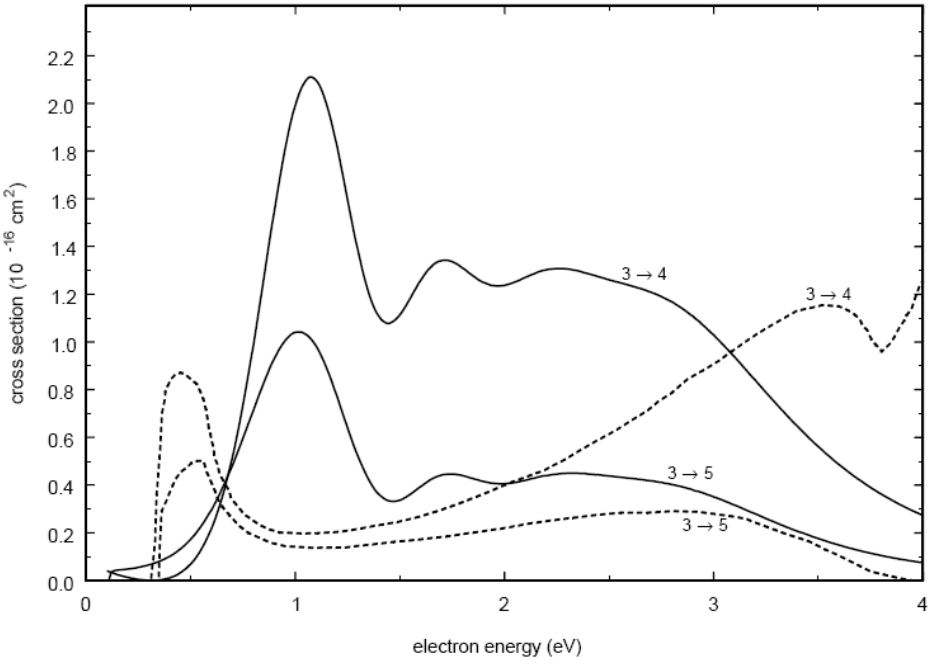

Figure 3. VE cross sections for the representative transitions $v_i \rightarrow v_f = 3 \rightarrow 4$ and 5. Solid curves, calculations using our model 2; dashed curves, calculations of the classical model, [10].

Summarizing this section, we have obtained a better fit to the differential VE cross sections of [2] using our model 2, which corresponds to the use of an *ab initio* calculated anion potential curve, than with model 1 which uses the previously published curve of [1]. We have found a large difference in magnitudes of the classical and present, quasiclassical, cross sections. This is due to the different nuclear probability distributions of the two theories.

4. Dissociative attachment

In Figure 5 our present calculations of the temperature-averaged DA cross sections at a vibrational temperature of 300 K are shown using both models 1 and 2. In the figure we compare our calculations with the swarm measurements of Spyrou and Christophorou [3] and with the beam measurements of Underwood-Lemons *et al.* [4].

First, we notice the large difference in the magnitudes of the calculations of the two models. The peak magnitude corresponding to model 1 is about 0.21×10^{-16} cm^2 whereas for model 2 it is about 0.03×10^{-16} cm^2. Also, the position of the peak corresponding to model 1 is at an electron energy of about 1.25 or 1.3 eV and for model 2 it is at about 1.4 or 1.5 eV. Both of these differences can be attributed to the higher survival probability of the resonance for model 1 as compared with model 2. These differences demonstrate the large effects that small changes in the anion potential curve can have on the DA cross sections. Therefore, it is very important to have accurate knowledge of the anion curve. We see from Figure 5 the calculations of model 2, which correspond to the use of our *ab initio* anion curve, agree much better with the magnitudes of available experimental measurements than the calculations using model 1.

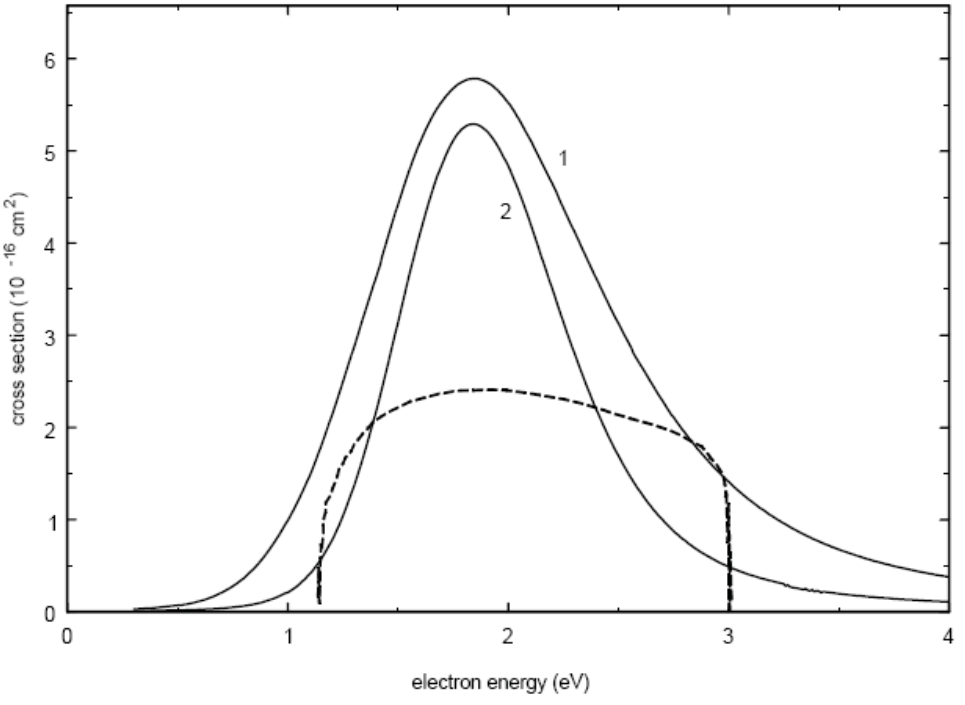

Figure 4. Summed VE cross sections for the transitions from $v = 0$ to $v = 1$ through 12. Solid curves, calculations using models 1 and 2, as indicated; dashed curve, calculations of the classical theory, [10].

In Figure 6(*a*) we compare our calculations using model 2 with the recent experimental data of Hahndorf *et al.* [1] at vibrational temperatures of 300 and 800 K. These measurements are relative, but the magnitude has been adapted from [3, 4] as described in [9]. The most striking feature of the DA cross sections at 800 K is the appearance of a large threshold peak near 0 eV. This sharp peak arises because the higher vibrational states of the neutral molecule are more populated at higher temperatures. Vibrational states with energies equal to or greater than the energy at the crossing point have a threshold energy of 0 eV, and, for these vibrational states, the partial cross sections diverge. This phenomenon has been described in some detail for the CH_3Cl molecule in [12]. In the absence of the dipolar interaction the cross section diverges as $1/k$, where k is the electron wavenumber. However, if the dipolar interaction is included without account of rotational motion, as was done in our calculations, the cross section behaves as $k^{2\lambda-1}$ near 0 eV [29], where λ is the threshold exponent which can be obtained from solving the angular part of the Schrödinger equation in the dipole field. For CF_3Cl, at equilibrium internuclear distance, $\lambda \approx -0.0262$. This value will depend slightly upon the vibrational state v. The DA cross sections for CH_3Cl are much smaller than in CF_3Cl due to a larger vertical attachment energy for CH_3Cl, about 3.2 eV. However, the CH_3Cl DA cross sections exhibit a strong temperature dependence similar to that in CF_3Cl.

For electron energies in the range 0–0.8 eV our calculations underestimate the DA cross sections according to the data of Hahndorf *et al*. We should note that averaging of our results over the experimental energy distribution leads to substantial reduction of the peak. This discrepancy may mean that the crossing point of the neutral and anion curves occurs at an energy that is too high in

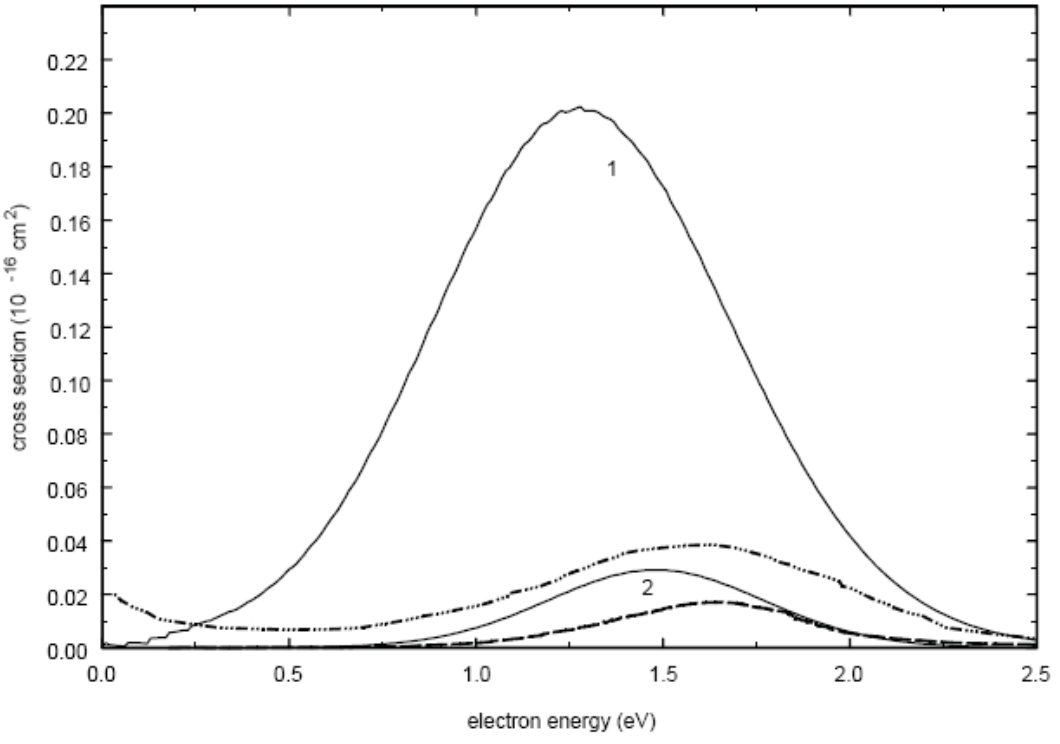

Figure 5. Temperature averaged DA cross sections at $T = 300$ K. Solid lines, our calculations using models 1 and 2, as indicated. Chain curve and dashed curve, swarm measurements of [3] and beam measurements of [4], respectively.

the case of model 2. In this case the Boltzmann-averaged cross sections for DA from the vibrational levels in this region, $v = 3$ and higher, might be too small. However, measurements of the absolute DA cross sections in the low energy region would be needed to clarify this.

At higher electron energies we see very good agreement between model 2 and the data of Hahndorf *et al*. The peak at 300 K which occurs at 1.4 or 1.5 eV nearly doubles in magnitude and broadens slightly as the temperature is increased to 800 K. This is again due to the greater population of the higher vibrational states at higher temperatures, which has been described in [1, 9].

In Figure 6(*b*) we show the results of the classical calculations of the DA cross sections at temperatures of 300 K and 800 K of Lehr and Miller [9]. The qualitative features of the classical calculations are in good agreement with the data of Hahndorf *et al*. However, the magnitudes are greater than those of the experimental data by a factor of 8. This discrepancy may be attributed again to the difference between the classical and quantum probability distributions for the nuclear motion. However, the anion potential used in the classical calculations is the same as that of model 1 and, as we have seen in our own calculations, a change in the anion curve might cause a large decrease in the classical DA cross sections. This possibility was also discussed in [9].

In Figure 7 we illustrate the dependence of the DA cross sections on the individual vibrational states, v, of the neutral molecule. Since vibrational states which lie above the crossing point diverge at 0 eV, as we have described above, we have calculated the average value of the cross sec-

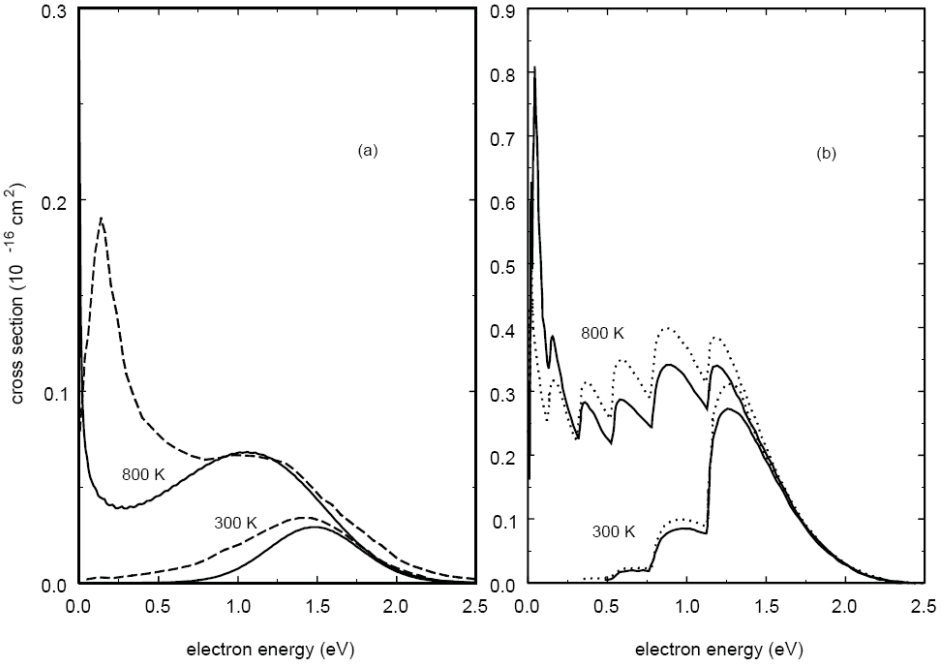

Figure 6. (*a*) Temperature averaged DA cross sections at temperatures of 300 and 800 K. Solid curves are our calculations using model 2 and dashed curves are the data of Hahndorf *et al.* [1], taken from [9]. (*b*) Results of the classical calculations of Lehr and Miller. The dashed and solid curves correspond to different parametrizations of the resonance width, see [9].

tions between $E_0 = 0$ and $E_1 = 0.1$ eV

$$\sigma_{\mathrm{av}} = \frac{1}{E_1}\int_0^{E_1} \sigma(E)\,\mathrm{d}E. \tag{7}$$

For the states which lie below the crossing point, we have plotted the peak values of the DA cross sections in Figure 7. We also show the peak values of the classically calculated cross sections of [9]. Since the classical calculations use the same potential curves as our model 1, we see a large increase in the magnitudes of the cross sections for $v = 5$ and 6. The calculations of model 2 show the increase occurring at $v = 9$ and 10, corresponding to the crossing of the neutral and our *ab initio* anion curves. For vibrational states lying above the crossing point we see a sharp decrease in the magnitude from the maximum value, after which the DA cross sections show relatively little dependence upon v. The classical cross sections show a monotonic decrease in the cross sections for higher v, whereas our calculations show some small variations. This difference, once again, is due to the difference between the classical and quantum methods of describing the nuclear motion. Classically, the velocity of the nuclei rises with v and consequently the DA cross sections will decrease with the rising velocity, see [9]. In our calculations the probability for capture of the electron depends upon the overlap between the vibrational wavefunction for a particular v and the continuum wavefunction. This overlap may exhibit slight variations for different v, as we see in Figure 7. Külz *et al.* have observed the large increase in the cross sections as a function of v for Na_2 [30, 31]. However, they did not observe a large decrease for states lying above the crossing point.

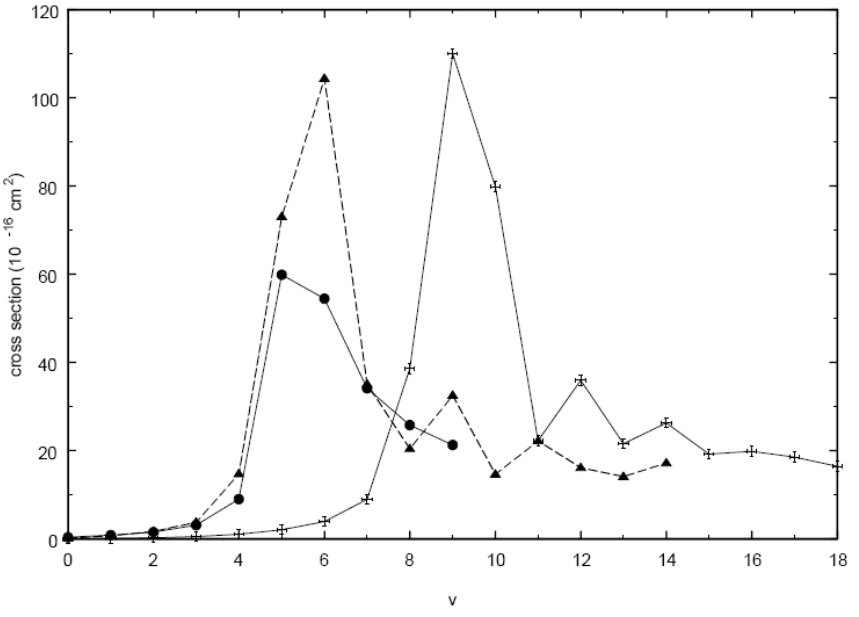

Figure 7. Dependence of DA cross sections on individual vibrational states *v*. Either the peak or the average value between 0 and 0.1 eV is plotted (see text). Triangles and crosses are calculations using models 1 and 2, respectively. Circles are peak DA cross sections of the classical model [9]. Lines connecting the individual points are meant only to help guide the eye.

5. Conclusion and summary

We have used the resonant *R*-matrix theory to calculate electron–molecule cross sections for both VE and DA in CF_3Cl. We have used two models based upon Morse parametrizations of two different anion potential curves. Model 1 corresponds to the curve of [1] and previously used in [9, 10] to calculate low energy electron scattering cross sections for CF_3Cl using a classical model. We have found that this potential gives DA cross sections which are much larger than experimental measurements. In order to improve our results and to put our theory on a more *ab initio* footing we have calculated points on the anion potential surface using quantum chemistry codes and fit the Morse function to these points yielding our model 2. Using this calculated curve leads to DA cross sections which agree well with experimental measurements. This results mainly because the anion potential curve in model 2 goes through the Franck–Condon region less steeply and the crossing point of the neutral and anion curves occurs at a higher energy than in model 1.

We have compared our calculations with the classical theory of [9, 10]. We obtain VE cross sections that are larger in magnitude than the classical theory and obtain DA cross sections that are smaller. These differences seem to be caused mainly by the fact that we use a quantum mechanical probability distribution for the nuclear separation whereas the model of [9, 10] uses a completely classical distribution.

The results obtained and described here have some similarities with those for CH_3Cl. In both molecules we see a large rise in the cross section at the 0 eV threshold and a broad peak at higher energies due to the temporary anion state which affects the ν_3 C–Cl mode. The magnitude of the cross sections for CH_3Cl are much smaller than for CF_3Cl due to the different vertical attachment energies

of the two molecules. However, the peak in the cross section for CH_3Cl rises more dramatically than in CF_3Cl. This makes the DA cross section for CH_3Cl very sensitive to the experimental environment. In particular, as mentioned above, the DA cross sections for CH_3Cl rise dramatically when it is placed on a surface or in bulk Kr [17–19]. A similar, but not as drastic, effect has been observed for CF_3Cl [20]. The semiempirical *R*-matrix method has been used previously to calculate the DA cross sections for CH_3Cl condensed onto a Kr surface [17, 18] and embedded in bulk Kr [19]. The results obtained in this paper would allow a similar theoretical description for the CF_3Cl molecule.

Acknowledgments

The authors are grateful to Professor P. D. Burrow for critical reading of the manuscript. This work was supported by the National Science Foundation through grant numbers PHY-9509265 and PHY-9801871.

References

[1] Hahndorf I, Illenberger E, Lehr L, and Manz J 1994 *Chem. Phys. Lett.* **231** 460
[2] Mann A and Linder F 1992 *J. Phys. B: At. Mol. Opt. Phys.* **25** 1621
[3] Spyrou S M and Christophorou L G 1985 *J. Chem. Phys.* **82** 2620
[4] Underwood-Lemons T, Gergel T J, and Moore J H 1995 *J. Chem. Phys.* **102** 119
[5] Jones R K 1986 *J. Chem. Phys.* **84** 813
[6] Kühn A and Illenberger E 1990 *J. Chem. Phys.* **93** 357
[7] Verhaart G J, Van Der Hart W J, and Brongersma H H 1978 *Chem. Phys.* **34** 161
[8] Illenberger E, Scheunemann H-U, and Baumgartel H 1979 *Chem. Phys.* **37** 21
[9] Lehr L and Miller W H 1996 *Chem. Phys. Lett.* **250** 515
[10] Lehr L, Manz J, and Miller W H 1997 *Chem. Phys.* **214** 301
[11] Chutjian A, Garscadden A, and Wadehra J M 1996 *Phys. Rep.* **264** 393
[12] Fabrikant I I 1991 *J. Phys. B: At. Mol. Opt. Phys.* **24** 2213
[13] Fabrikant I I 1994 *J. Phys. B: At. Mol. Opt. Phys.* **27** 4325
[14] Pearl D M, Burrow P D, Fabrikant I I, and Gallup G A 1995 *J. Chem. Phys.* **102** 2737
[15] Fabrikant I I, Pearl D M, Burrow P D, and Gallup G A 1994 *Electron Collisions with Molecules, Clusters and Surfaces* ed H Ehrhardt and Z A Morgan (New York: Plenum)
[16] Sambe H, Ramaker D E, Deschenes M, Bass A D, and Sanche L 1990 *Phys. Rev. Lett.* **64** 523
[17] Sanche L, Bass A D, Ayotte P, and Fabrikant I I 1995 *Phys. Rev. Lett.* **75** 3568
[18] Ayotte P, Gamache J, Bass A D, Sanche L, and Fabrikant I I 1997 *J. Chem. Phys.* **106** 749
[19] Fabrikant I I, Nagesha K, Wilde R, and Sanche L 1997 *Phys. Rev.* B **56** R5725
[20] Nagesha K and Sanche L 1996 *Phys. Rev. Lett.* **78** 4725
[21] Lane A M and Thomas R G 1958 *Rev. Mod. Phys.* **30** 257
[22] Bishop D M and Cheung L M 1982 *J. Phys. Chem. Ref. Data* **11** 119
[23] Schneider B I, Le Dourneuf M. and Burke P G 1979 *J. Phys. B: At. Mol. Phys.* **12** L365
[24] Kazansky A K and Yelets I S 1984 *J. Phys. B: At. Mol. Phys.* **17** 4767
Kalin S A and Kazansky A K 1990 *J. Phys. B: At. Mol. Opt. Phys.* **23** 4377
[25] Fabrikant I I 1991 *Phys. Rev.* A **43** 3478
[26] Schmidt M W *et al.* (GAMESS Version 18) 1993 *J. Comput. Chem.* **14** 1347–63
[27] Asubiojo O I, Blair L K, and Brauman J I 1975 *J. Am. Chem. Soc.* **97** 6685
[28] Bertran J, Gallardo I, Moreno M, and Savéant J-M 1992 *J. Am. Chem. Soc.* **114** 9576
[29] Fabrikant I I 1977 *Sov. Phys.–JETP* **46** 693
[30] Külz M, Kortyna A, Keil M, Schellhaass B, and Bergmann K 1993 *Phys. Rev.* A **48** R4015
[31] Külz M, Keil M, Kortyna A, Schellhaass B, Hauck J, Bergmann K, Meyer W, and Weyh D 1996 *Phys. Rev.* A **53** 3324